Progress in Nuclear Energy 108 (2018) 204–213

Contents lists available at ScienceDirect

Progress in Nuclear Energy

journal homepage: www.elsevier.com/locate/pnucene

Investigation of single bubble rising velocity in LBE by transparent liquids similarity experiments

Chaodong Zhang[a,b], Danna Zhou[a,*], Rongyuan Sa[a], Qingsheng Wu[a]

[a] Key Laboratory of Neutronics and Radiation Safety, Institute of Nuclear Energy Safety Technology, Chinese Academy of Sciences, Hefei, Anhui, 230031, China
[b] University of Science and Technology of China, Hefei, Anhui, 230026, China

ARTICLE INFO

Keywords:
Lead-based reactor
SGTR
Bubble migration
Bubble rising velocity

ABSTRACT

Based on the pool type lead-based reactor, the two-phase flow phenomenon remains a longstanding challenge in a Steam Generator Tube Rupture (SGTR) scenario. In order to investigate the bubble rising velocity in opaque liquid Lead Bismuth Eutectic (LBE), experiments were carried out by injecting argon gas into four transparent liquids (water, glycerol, alcohol and FC-3283). The appropriate drag coefficient of a single bubble was obtained by dimensionless Eötvos number under different liquids. For bubble equivalent diameter from 4 mm to 6 mm, the bubble flow located in the regime of surface tension dominant, where the bubble terminal rising velocity tended to a value almost independent of the bubble diameter. The single bubble rising velocity remained about 0.252 m/s to 0.274 m/s in gas-liquid metal bubbly flow. An appropriate modified correlation was recommended to roughly forecast the single bubble terminal rising velocity in two phase flow with high liquid-to-gas density ratio. These data can provide a reference on analyzing bubble migration process under accident condition.

1. Introduction

Lead cooled Fast Reactor (LFR) is one of the six candidates selected by the generation IV, which has good capability for the efficient utilization of uranium resource and the transmutation of long-lived radioactive waste (Tuček et al., 2006; Moisseytsev and Sienicki, 2008; Wu et al., 2016a; Wu, 2016a). LFR is an innovative nuclear reactor having characteristics of inherent safety, economics and sustainability and it has been studied by some countries that use nuclear power. In 2006, the ELSY (European Lead-cooled System) project was funded by the EC (European Community), which is aimed at demonstrating the possibility of designing a competitive and safe pool-type reactor (Cinotti et al., 2011). In 2010, The LEADER (Lead-cooled European Advanced Demonstration Reactor) project was initiated to develop an enhanced concept for a large-size LFR as part of the 7th Framework Programme. Presently, a small LFR demonstrator, the development of ALFRED (Advanced Lead-cooled Fast Reactor European Demonstrator) project is underway (Frogheri et al., 2015). In Russia, the works on LFR have been in progress. The experimental and industrial prototype power unit with SVBR-75/100 had lead-bismuth eutectic coolant, which was developed for the nuclear submarine (Zrodnikov et al., 2011, 2006). In China, the Institute of Nuclear Energy Safety Technology (INEST/FDS Team), Chinese Academy of Sciences carried out R&D activities about advanced reactor system including reactor conceptual design and safety analysis (Wu and FDS team, 2006, 2007a, b, c; Qiu et al., 2000; Wang et al., 2015a; b; Wu et al., 2011, 2016b; Wu, 2009), reactor material and key technologies (Huang et al., 2011; Huang and FDS team, 2014; Huang, 2017; Wu et al., 2010). China LEAd-based Reactor (CLEAR) was selected as the reference reactor for the Accelerator Driven subcritical System (ADS) program, which is being performed by INEST/FDS Team. The objective of the first stage is to complete the conceptual design and engineering design for China LEAd-based Research Reactor named CLEAR-I with ~10MW thermal power (Wu et al., 2014, 2015, Wu, 2016b).

The LFR is usually designed as pool type reactor (Cinotti et al., 2007) which has the Primary Heat Exchangers (PHXs) or Steam Generators (SGs) directly into the primary vessel. In such a configuration, an important safety concern due to the Steam Generator Tube Rupture (SGTR) scenario cannot be ignored. It is considered one of the main accidents as it could result in a loss of the barrier between the primary and the secondary coolants. The secondary coolant (water) could blast into the primary coolant (liquid metal) in a postulated SGTR accident (Wang et al., 2008; Gu et al., 2015). The high pressure and sub-cooled water directly contacts with the high temperature and low pressure liquid metal coolant (350 °C, 0.1MPa). The water in the SGs tube boils violently and forms steam-liquid metal two-phase flow via the rupture site because of rapid depressurization and superheating (Pesetti et al., 2015). For the dispersed flow regime, the steam bubbles would

* Corresponding author.
E-mail address: danna.zhou@fds.org.cn (D. Zhou).

https://doi.org/10.1016/j.pnucene.2018.05.011
Received 30 August 2017; Received in revised form 6 May 2018; Accepted 14 May 2018
Available online 05 June 2018
0149-1970/

therefore be entrapped and carried downward by the primary coolant flow when the downward velocity of circulation flow is higher than the bubble terminal rise velocity (Dinh, 2008). The steam migrated by the coolant flow into the core region is considered as a credible threat due to the potential effect of a significant positive void worth (Wang et al., 2008).

As for the rising characteristics of single bubble in viscous liquids, some experimental and theoretical works have been performed in previous study. Peebles and Garber (Peebles and Garber, 1953) described an initial phase of an extensive investigation on gas-bubble behavior. Kupferberg et al. (1969) proposed a theoretical model to describe the bubble formation at an orifice. Ishii and Chawla, (1979) carried out the bubble migration experimental study by injecting gas into a series of transparent liquid and presented the empirical relation between the bubble drag coefficient and dimensionless number *Re* and *Eo*. Ziqi et al. (2010) conducted a gas-glycerol two phase flow experiment to investigate the rising behavior of single bubble. However, most of these studies were focused on the air bubble rising behaviors in transparent liquid. Several empirical correlations to understand and predict bubble velocity have been proposed in the literatures (Stokes, 1851; Mendelson, 1967). Unfortunately, the applicability of these correlations may be limited to specific conditions. Mishima et al. (1999) performed a preliminary study on visualization and void fraction measurement of gas-liquid metal two-phase flow by using neutron radiography technique. Sibamoto et al. (2002) investigated the subcooled water jet injection into liquid melt by using high-frame-rate neutron radiography. Saito et al. (Saito et al., 2005a, b) studied the liquid metal two-phase flows in metallic vessels by using neutron radiography and electrical conductivity probe. Suzuki et al. (2003) simulated the gas-liquid metal flows by using the SIMMER-III code. Chakraborty et al. (2015) carried out numerical simulations of the gas bubble formation in a quiescent high-density liquid metal. The volume of the detached bubble was evaluated for various Weber numbers and the transition of period-1 to period-2 with pairing and coalescence was shown on a Weber-Bond numbers map. However, due to opaqueness of liquid metal, the experimental data were not very clear and the database for bubble in liquid metal used for the validation and verification on the numerical code has been insufficient. Further research for bubble migration in liquid metal is needed.

In the present study, a series tests have been conducted to investigate the flow characteristics of argon bubble rising in different fluids (water, glycerol, alcohol and FC-3283) by utilizing visualization technology. In order to predict the bubble rising behaviors in liquid metal, some suitable dimensionless parameters were identified by some similarity experiments. To achieve this aim, a two-phase flow experimental apparatus was set up, and the single bubble rising velocity in transparent fluid was obtained by visualization method taken with a high-speed camera. The single bubble rising velocity was forecasted by dimensionless Eötvos number analysis and an appropriate modified correlation was recommended for bubble equivalent diameter from 4 mm to 6 mm in gas-liquid metal bubbly flow. This study will provide good reference for analyzing bubble migration process in liquid metal and optimizing the reactor design.

2. Experimental apparatus and procedure

The schematic view of the test apparatus is illustrated in Fig. 1, which consists of a rectangular-duct section, a high-speed camera (type: PCO. dimax HD), two strobe-flash lights, a gas flow meter and an image acquiring system (Camware software). The cuboid test tank is made up of stainless steel of 250 × 250 × 800 mm. In order to visualize the motion process of bubbles, two Plexi-glass observation windows are installed in the front and rear of the test tank. Water, glycerol, alcohol and FC-3283 are used as test fluids. The physical properties of the four testing fluids at ambient temperature and liquid LBE at 350 °C are shown in Table 1. The camera with two strobe-flash lights is used to capture the detailed bubbles. A rectangle semitransparent glass plate diffuser is located between the strobe-flash light and test tank to obtain a dispersive uniform light source and white background.

At the present experiments, the liquid height from the nozzle was controlled more than 300 mm and the injecting gas flow rate was about 0.03–1 L/min to ensure generating a single bubble. The bubbles were formed at the nozzle immersed at the stagnant liquid and then moved upward at the effect of buoyancy. The nozzle size can be replaced and the diameters used are 2, 4 and 6 mm, respectively. The argon was supplied by a high-pressure gas tank with the volume about 40 L through a valve, a pressure reducer and a gas flow meter. The pressure in gas tank was about 2–12MPa and through the pressure reducer the pressure reduced to 0–0.2 MPa as the test pressure. The temperature of the testing liquid was ambient temperature ant the pressure of the testing liquid was atmospheric pressure.

The data of bubble rising behavior in the test liquid were recorded by using the high-speed camera. It is possible to record frame rate at 100755 fps through this system. In the present tests, the maximum frame rate of 6017 fps at a resolution of 288 × 948 pixel was selected. The recording time was about 3 s and it could obtain the detail image of bubble migration upward. A sequence of bubble motion images was analyzed by the image digital recognition code programmed by MATLAB software. This code can recognize image information of each bubble and provide the velocity and the size of a single bubble. The terminal rising velocity of a single bubble is the average value derived from the images of bubble stable path. The details of the experimental conditions are indicated in Table 2.

3. Results and discussions

3.1. Bubble rising velocity measurement

The experiments with 2–4 mm nozzle diameter have been carried out by injecting gas into water, glycerol, alcohol, FC-3283 and the single bubble rising process was obtained. Fig. 2shows the single bubble flow patterns at four fluids with nozzle diameter 4 mm. It clearly shows that the bubble grew as a sphere type at the nozzle, and it elongated vertically. Then, the bubble became a prolate spheroid shape and finally the bubble detached from the nozzle tip and float up. The single bubble generated during this condition without any coalescent. The bubble shape transformed form spherical to ellipsoidal and the trend was almost a straight line up during the rising process. It is evident that the rotation phenomena happened when bubble rising in liquid. The bubbles were deformed and some irregular shapes were appeared at the top of the flow path. This happens mainly because the bubbles motion under the action of the main forces including gravity, buoyancy and drag forces. From Fig. 2(a), it is important to highlight that the bubbles lifted up in water with ellipsoidal type. However, the bubble type almost remained spherical when bubble rose in glycerol as shown in Fig. 2(b). The bubble type had severe deformation in alcohol and FC-3283 as shown in Fig. 2(c) and (d).

In order to calculate the bubble equivalent diameter, the minor axis (a) and the major axis (b) of the single bubble are defined as follow (see Fig. 3).

The bubble equivalent diameter, d_e, is given in terms of bubble volume V_b, by

$$d_e = \left(\frac{6V_b}{\pi}\right)^{1/3} \tag{1}$$

where bubble volume, V_b, is calculated by

$$V_b = \frac{\pi b a^2}{6} \tag{2}$$

The minor axis (a) and the major axis (b) of the single bubble were obtained by image analysis.

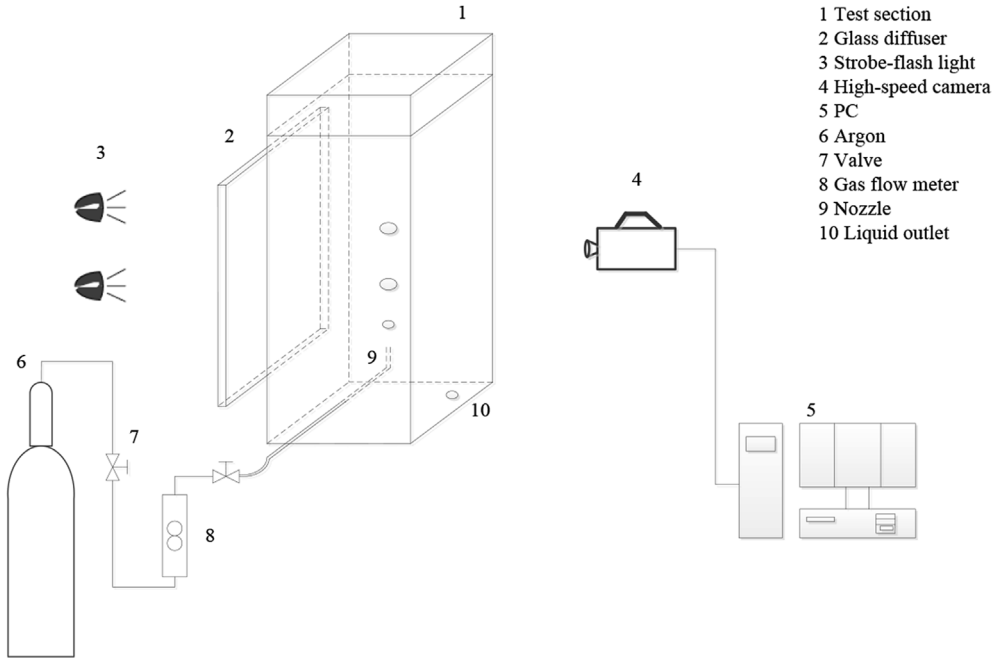

Fig. 1. Schematic view of test apparatus.

Table 1
Physical properties of the test fluids at ambient temperature (20 °C).

Property	Symbol	Water	Glycerol	Alcohol	FC-3283	LBE(350 °C)
Viscosity (mPa·s)	μ	1.00	9.48	1.07	1.36	1.66
Surface tension (N/m)	σ	0.072	0.0564	0.022	0.015	0.395
Density (kg/m^3)	ρ_l	998	1054	789	1820	10271

Table 2
Details of the experimental conditions.

Test material	Water, glycerol, alcohol and FC-3283
Nozzle diameter (mm)	2, 4, 6
Gas flow (L/min)	0.03–1
Test pressure (MPa)	0–0.2
Test temperature (°C)	20 (ambient temperature)
Frame speed of camera (fps)	6017

The original images of bubbles of different sizes in four working liquids are as shown in Fig. 4. It should be mentioned that, the bubble approximately treated as sphere and ellipsoid including the deformed bubbles. The bubble equivalent diameter was calculated by Eq. (1). The maximum bubble equivalent diameter in water, glycerol, alcohol and FC-3283 is about 7.5 mm, 6.6 mm, 6.0 mm and 7.5 mm, respectively and the minimum one is about 2.5 mm formed in alcohol. The bubble shape in glycerol was almost sphere and ellipsoid in alcohol and water. The bubble shape in liquid FC-3283 was badly deformed and it transited to cap-shape. Grace, (1976) proposed a bubble-shape map based on dimensionless Morton (Mo), Eötvos (Eo) and Reynolds (Re) number to describe the bubble shape. In LBE case since the density is very high (~10000 kg/m^3), the Mo number is very low and it is about 10^{-13}. According to the physical properties in Table 1, the order of Mo number of these liquid is $(Mo)_{LBE} < (Mo)_{FC\text{-}3283} < (Mo)_{water} < (Mo)_{alcohol} < (Mo)_{glycerol}$. Referring to the bubble-shape map, it can be concluded that the single bubble shape in liquid LBE will be the ellipsoid transited to cap-shape or the cap-shape.

The bubble motion process in water at different time with 2 mm nozzle inner diameter is shown in Fig. 5. According to the rising height of one single bubble and time interval, the bubble rising velocity can be obtained. It can be noted that the bubble rising height is nearly constant after the time is about 0.32 s. It means the bubble rising velocity will maintain constant.

The barycenter of each bubble is defined by

$$X = \frac{1}{N}\sum_{i}^{N} x_i, \quad Y = \frac{1}{N}\sum_{i}^{N} y_i \tag{3}$$

where X is the horizontal coordinate of mass center, Y is the vertical coordinate of mass center, x_i is the horizontal coordinate of pixel, y_i is the vertical coordinate of pixel, i is the ith bubble, and N is the total number of pixels for a bubble area.

The bubble rising velocity can be calculated by

$$V = \frac{\Delta h}{\Delta t} \tag{4}$$

where V is the single bubble rising velocity, $\triangle h$ is the rising height of one single bubble between two vertical coordinate, $\triangle t$ is the time between two images.

Fig. 6 (a), (b) (c) and (d) show the experimental results of the bubble rising velocity with the vertical distance from the gas nozzle, in which the average values are designated. It is found from these figures that the bubble rising velocity increased gradually from the vicinity of the nozzle orifice at first, and then reached the stable value at about 1/3 height of the liquid level (~90 mm). Finally, the terminal rising velocity stays with small fluctuations, where the forces are balanced between the drag and buoyancy produced by the low gas density and high liquid density. The average terminal rising velocity is about 248 mm/s in water, 231 mm/s in glycerol, 218 mm/s in alcohol and 197 mm/s in FC-3283, respectively.

The experimental uncertainty for the calculating of the bubble velocity is given by Eq. (5) (Celata et al., 2007)

$$\triangle V = \sqrt{\left(\frac{\partial V}{\partial P_1}dP_1\right)^2 + \left(\frac{\partial V}{\partial P_2}dP_2\right)^2 + \left(\frac{\partial V}{\partial \Delta t}d\Delta t\right)^2 + \left(\frac{\partial V}{\partial s}ds\right)^2} \tag{5}$$

where P_1 and P_2 are the barycenter positions (pixel), s is the scale factor (mm/pixel).

The bubble rising velocity $V = \triangle h/\triangle t = (Y_2 - Y_1)/\triangle t = (P_2 s - P_1 s)/\triangle t$, so that

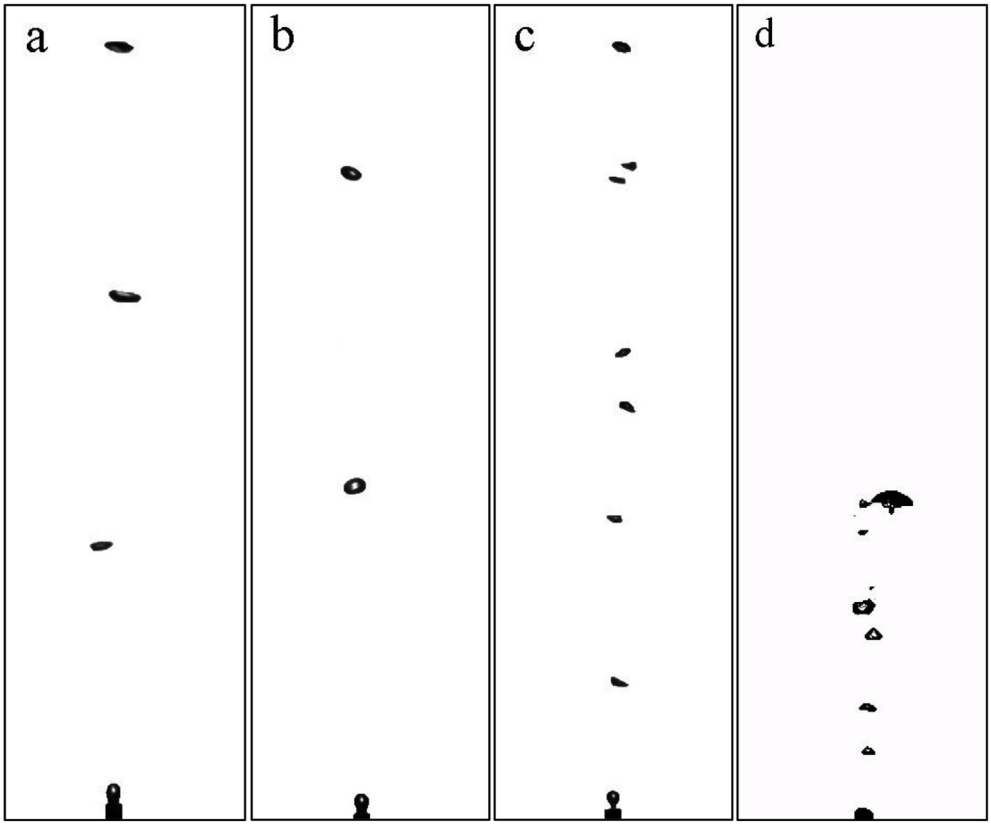

Fig. 2. Single bubble flow patterns at different fluids (d_n = 4 mm).

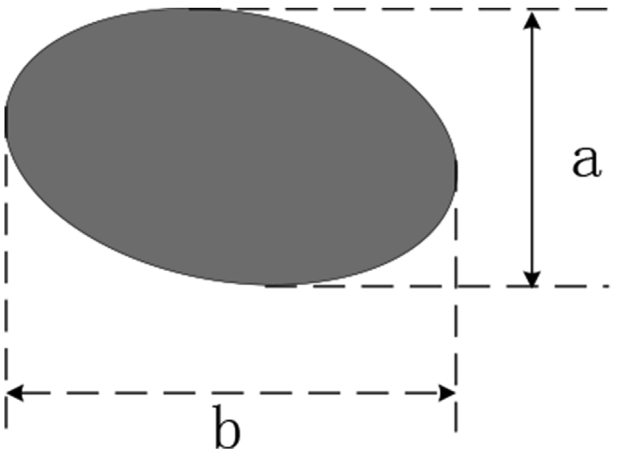

Fig. 3. Bubble minor axis (a) and the major axis (b).

$$\frac{\partial V}{\partial P_1} = -\frac{s}{\triangle t},\quad \frac{\partial V}{\partial P_2} = \frac{s}{\triangle t},\quad \frac{\partial V}{\partial \triangle t} = -\frac{(P_2 s - P_1 s)}{(\triangle t)^2},\quad \frac{\partial V}{\partial s} = \frac{P_2 - P_1}{\triangle t}$$

In the present case, for the instantaneous velocity we have:

(1)Δt = 1/fps = 1/6017 = 1.6×10^{-4} s, $d\Delta t = 10^{-6}$ s

(2) $dP_1 = dP_2 = \pm 1$ pixel, assuming a maximum error in the definition of the contour of the bubble yields;

(3) ds =0.004 mm/pixel, the reference condition is given by a scale-plate with 50 mm length and the measurement was repeated many times.

In present study, the terminal velocity is averaged on a path of 2/3of the maximum one, we have,

$$P_1 = P(Y_{max}/3);\quad P_2 = P(Y_{max});\quad \Delta t = \frac{2}{3}t_{\text{tot}}$$

The relative error in measurement can be obtained as $E_r = (\triangle V/V) \times 100\%$. The resulting relative error of bubble terminal rising velocity is about 1.28% in water, 1.38% in glycerol, 1.46% in alcohol and 1.55% in FC-3283, respectively.

The major uncertainty in the bubble equivalent diameter is the measurement of the bubble axis in the digital image system. Assuming a maximum error of ± 1 pixel in the definition of the axis of the bubbles that the average uncertainty in the equivalent diameter measurement is about 3.73%–6.88% for water, 3.90%–5.81% for glycerol, 4.67%–11.20% for alcohol and 4.72%–12.40% for FC-3283.

3.2. Terminal rising velocity calculationq

When the bubble moved from the nozzle in a liquid with the effect of the gravity, buoyancy and drag force, the velocity would hold at a constant rate after the balance condition established. Based on the force equilibrium relationship, the equation can be expressed as

$$\rho_l g\frac{\pi d_e^3}{6} = \rho_g g\frac{\pi d_e^3}{6} + \frac{1}{2}C_D\rho_l V_T^2 A \tag{6}$$

where ρ_l, ρ_g, g, d_e, C_D, V_T and A are liquid density, gas density, gravitational acceleration, bubble equivalent diameter, drag coefficient, single bubble terminal rising velocity and the bubble cross-sectional area, respectively.

For turbulent region and larger bubble conditions, an empirical correlation proposed by Harmathy (1960) to calculate the single bubble terminal rising velocity. This correlation is expressed as

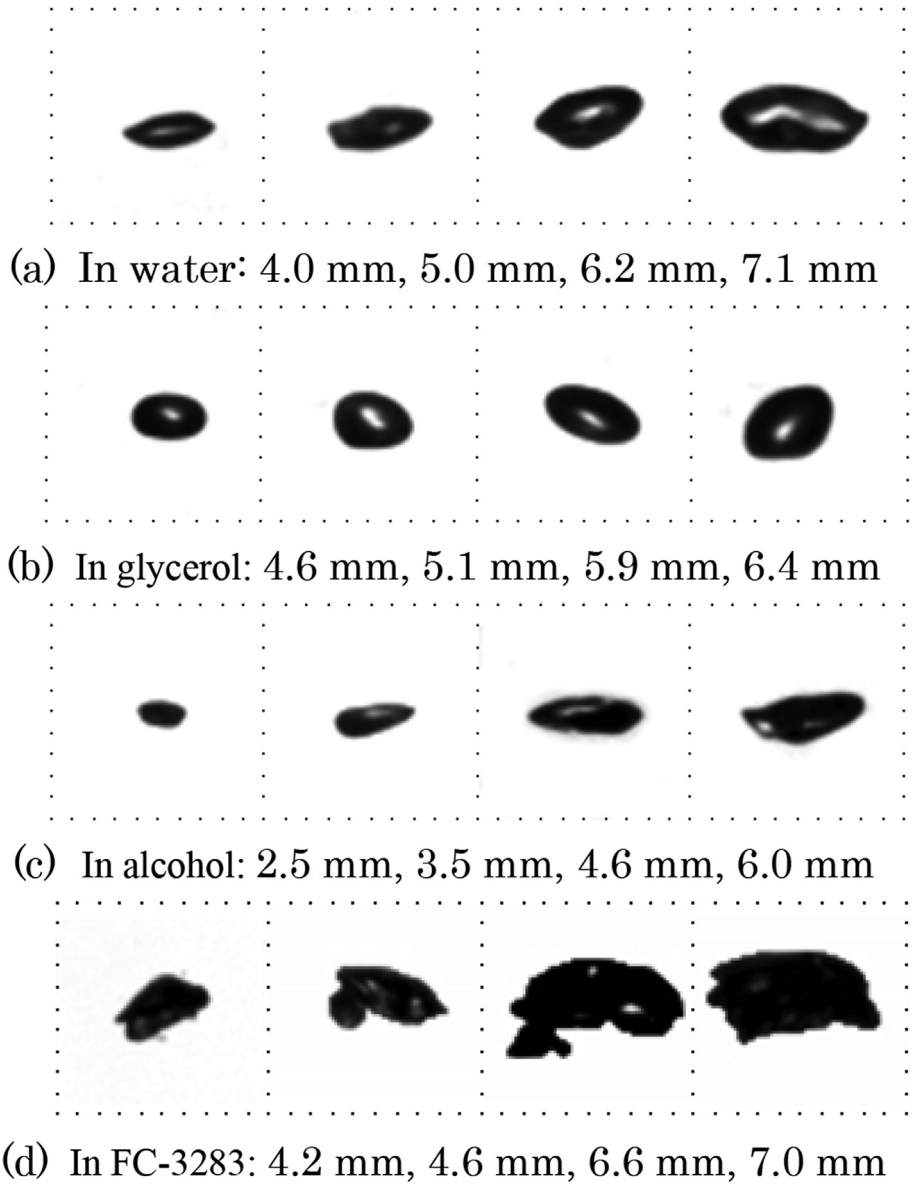

Fig. 4. Images of bubbles of various equivalent diameters in water, glycerol, alcohol and FC-3283.

$$V_T = 1.53\left(\frac{g\sigma}{\rho_l}\right)^{0.25} \quad (3.10G_1^{-0.25} < Re \text{ or } 5.75 < G_2) \tag{7}$$

where σ and Re are liquid surface tension and Reynolds number, respectively. G_1 and G_2 are the dimensionless numbers and given by

$$G_1 = \frac{g\mu_l^4}{\rho_l\sigma^3}, \quad G_2 = \frac{gr_b^4V_T^4\rho_l^3}{\sigma^3} \tag{8}$$

where μ_l, r_b are liquid viscosity and bubble radius, respectively. The dimensionless number G_1 is 2.63×10^{-11}, 4.18×10^{-7}, 1.55×10^{-9}, 8.19×10^{-11}, respectively for the present testing fluids.

The single bubble terminal rising velocity with the bubble equivalent diameter is shown in Fig. 7. The data in the water, glycerol, alcohol and FC-3283 are presented in the same graph and the nozzle diameter of 2 mm, 4 mm and 6 mm had been used. For the present data, the Re is always 1133–1396 for water, 127–158 for glycerol, 472–911 for alcohol and 790–1977 for FC-3283, which accord with the Eq. (7) calculation conditions. As shown in these figures, full squares and triangles represent data with the nozzle diameter 2 mm and 6 mm and the open squares denote data with middle nozzle diameter 4 mm. We may see the bubble equivalent diameter exceeds the nozzle diameter when a bubble moved freely. The bubble terminal rising velocity tended to a value which was independent of the bubble equivalent diameter. As already observed for water data in Fig. 7 (a), the bubble equivalent diameters were about 3.5 mm–7.5 mm which was located in the regime of surface tension dominant (for gas-water system Eötvos number should be 0.25 to 40). In this condition, the bubble terminal velocity is governed by the inertia force and surface tension and it exhibits a slightly oscillating trend. The terminal velocity was about 248 mm/s for bubble equivalent diameters 3.5 mm–5.5 mm and the experimental results have shown appropriate agreement with the Harmathy empirical correlation. For bubble equivalent diameter 5.5 mm–7.5 mm, the terminal velocity was about 240 mm/s, which was slightly below the 3.5 mm–5.5 mm bubbles. The Harmathy empirical correlation predicted value tends slightly overestimated the experimental results. For glycerol data, the bubble equivalent diameters were about 4 mm–6.5 mm as shown in Fig. 7 (b). It is found that the terminal velocity trend remained a constant and independent of the bubble diameter. The Harmathy empirical correlation predicted value showed a good agreement with the experimental. Fig. 7 (c) shows the results of single bubble terminal velocity in alcohol versus the bubble equivalent diameter. This figure indicates that the

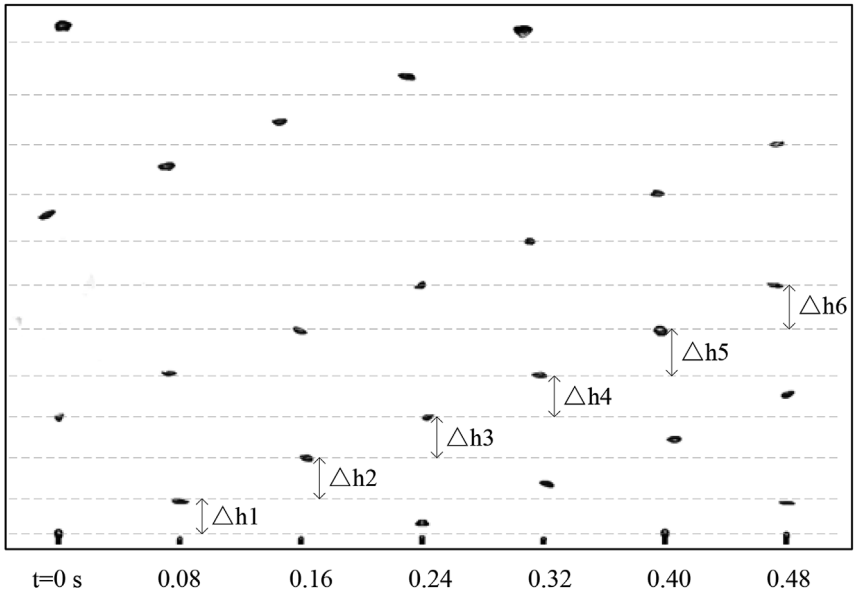

Fig. 5. Single bubble rising process in water.

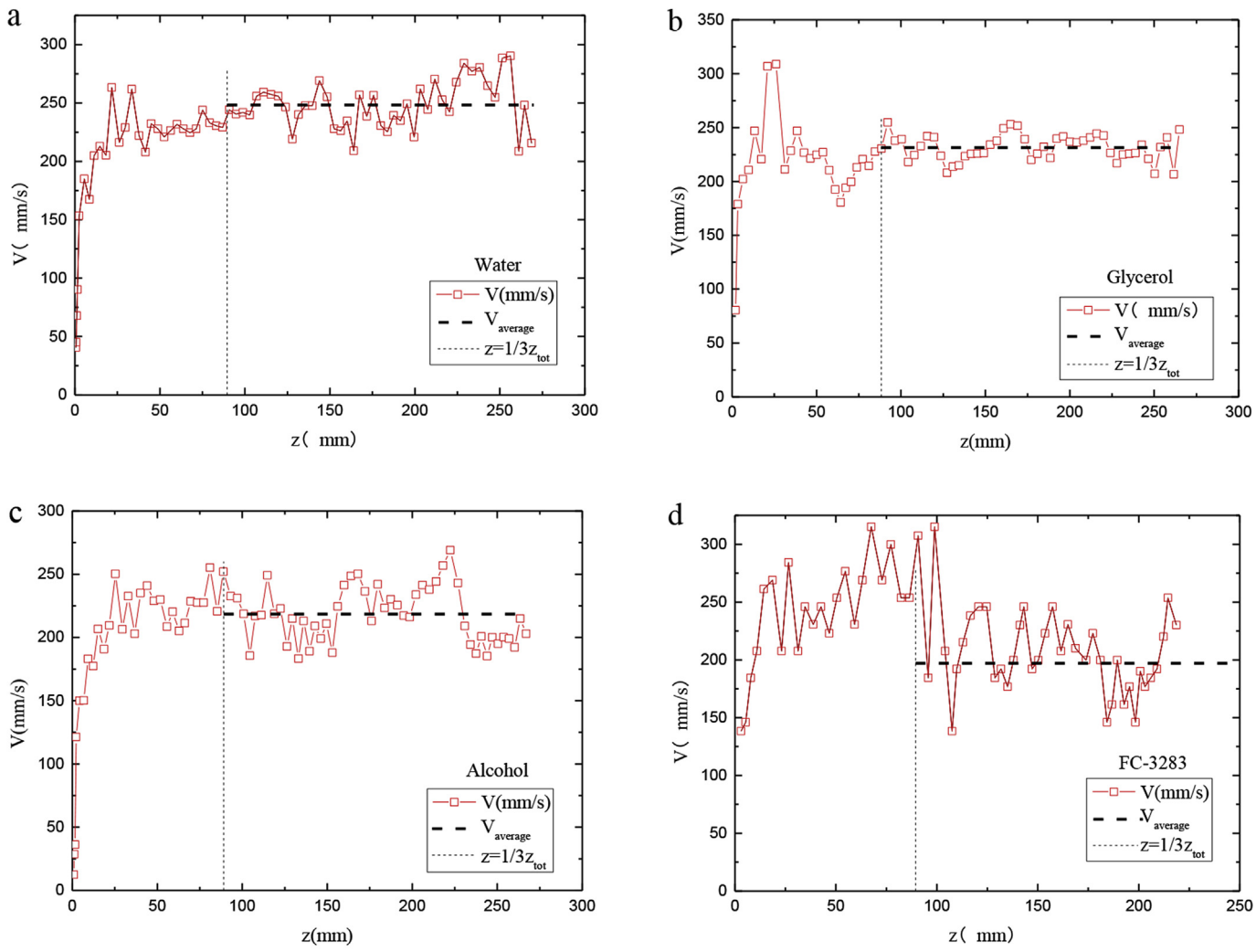

a: argon-water; b: argon-glycerol; c: argon-alcohol; d: argon-FC-3283

Fig. 6. Single bubble rising velocity at the bubble path (d_n = 2 mm).

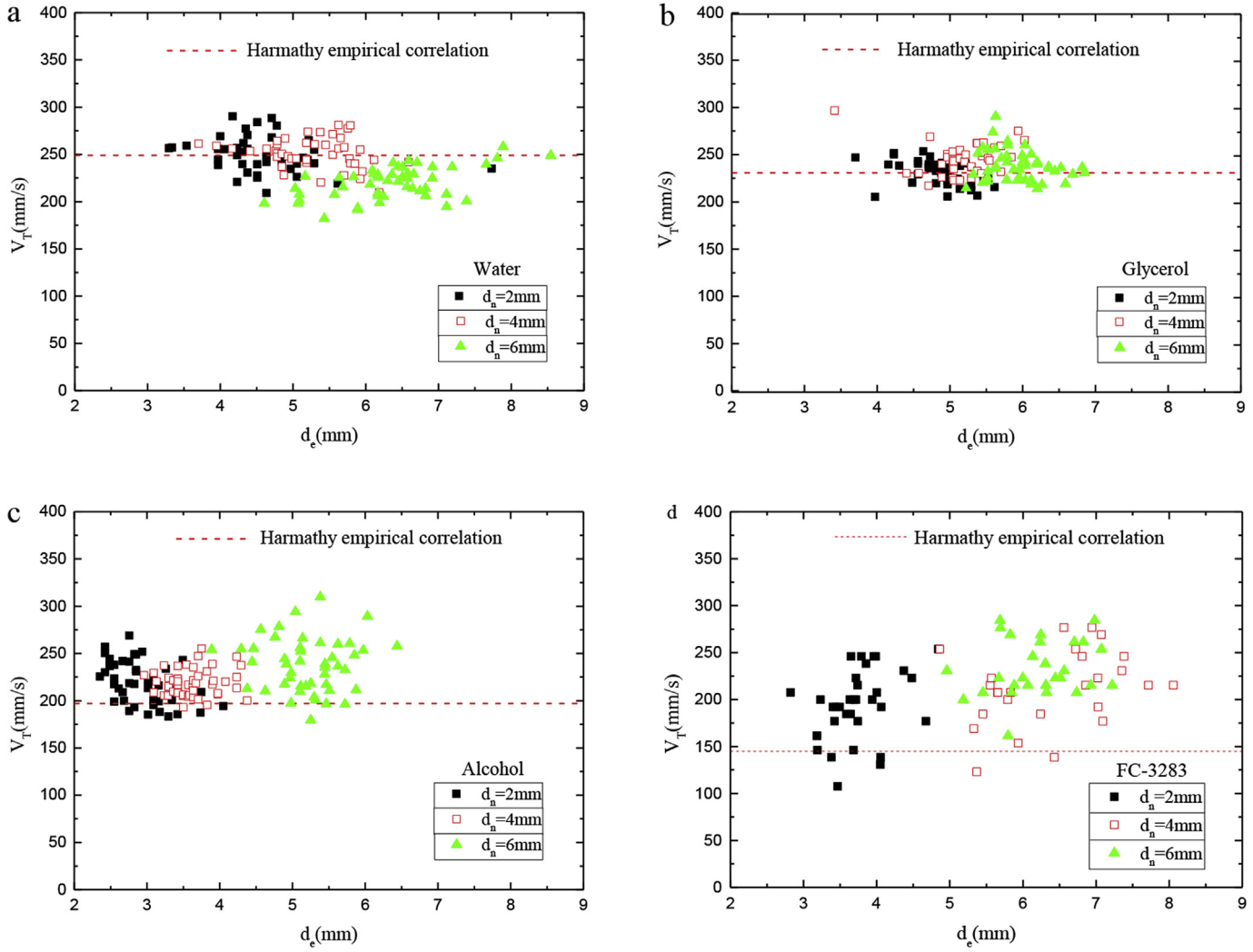

Fig. 7. Terminal velocity versus bubble equivalent diameter.

bubble equivalent diameter distribution was about 2.5 mm–6 mm. It is found that the bubble terminal velocity was about 220 mm/s and the Harmathy empirical correlation tends slightly underestimated the experimental results. Fig. 7 (d) shows the results of single bubble terminal velocity in FC-3283. The figure indicates that the bubble equivalent diameter distribution was about 3.0 mm–7.5 mm. It is found that the bubble terminal velocity was about 200 mm/s and the Harmathy empirical correlation tends slightly underestimated the experimental results. The information obtained from Fig. 7 (a) ~ (d) indicates that the bubble motion located in the surface tension dominant regime and bubble terminal velocity did not depend on the bubble diameter for equivalent diameter 4 mm–6 mm. The Harmathy empirical correlation Eq. (7) can be used to roughly forecast the single bubble rising velocity in this regime for water, glycerol, alcohol and FC-3283 system.

3.3. Terminal rising velocity prediction

In the analysis, it was recognized that large bubbles will be extremely deformed under the action of the surface tension which has a great influence on rising velocity. The density difference between liquid and gas phase affects the bubble buoyancy. The ratio of surface tension to density difference, in general, determines the large bubble terminal rising velocity and it increased with the increasing of the ratio.

In order to evaluate the terminal rising velocity V_T, we need to calculate the drag coefficient C_D. With the force equilibrium relationship between the buoyancy and the drag forces on a bubble, the drag coefficient can be calculated from Eq. (6).

$$C_D = \frac{\pi d_e^3 g}{3AV_T^2} \tag{9}$$

where A is the single bubble cross-sectional area, and it is obtained by a method of MATLAB image processing.

Previous studies (Suzuki et al., 2003) have shown that the drag coefficient C_D can be written as a function of dimensionless group:

$$C_D = f(Re, Eo, Mo) \tag{10}$$

For the surface tension dominant regime, Ishii and Chawla, (1979) first presented that the bubble drag coefficient could be simply expressed by *Eo*, and it is independent of *Re*, *Mo*. So, considering the present study, Eq. (10) can be rewritten by dimensionless Eötvos number.

$$C_D = f(Eo) \tag{11}$$

A typical experimental results of bubble drag coefficient versus

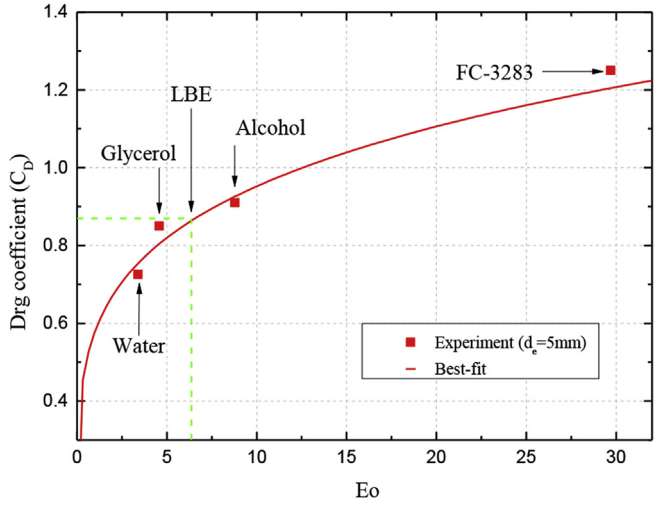

Fig. 8. Drag coefficient versus Eötvos number.

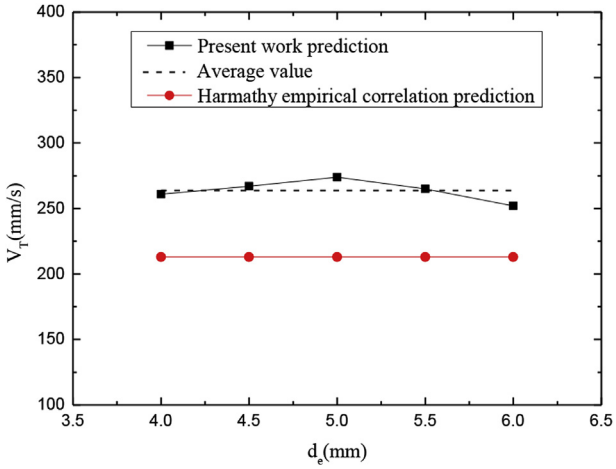

Fig. 9. Prediction of single bubble terminal rising velocity in liquid LBE (d_e = 4–6mm).

Eötvos number (d_e = 5 mm) for four different liquids (water, glycerol, alcohol and FC-3283) were shown in Fig. 8. The value of drag coefficient for a bubble was obtained by using Eq. (9), where the cross-sectional area A was calculated by average value corresponding to the bubble equivalent diameter with image recognition and the bubble terminal velocity was obtained by average experimental results. Full squares denote calculated values by Eq. (9) with 5 mm bubble equivalent diameter. The solid line represents the fitted curve for experimental results of four transparent liquids. As shown in this figure, the value of drag coefficient increased with the increasing of Eötvos number. This correlation is expressed as

$$C_D = 0.579\mathrm{Eo}^{0.216} \tag{12}$$

Due to the Eötvos number (6.37) of LBE between glycerol (4.58) and alcohol (8.79), we predict the bubble drag coefficient is about 0.87 with 5 mm equivalent diameter bubble moving in LBE by solving Eq. (12). The other values of drag coefficient in different equivalent diameters can be obtained by using the same method and the results are presented in Table 3.

Substituting $(C_D)_{LBE}$ into Eq. (6), the terminal rising velocity of a single bubble in liquid LBE can be calculated. Fig. 9 shows the prediction value of single bubble terminal rising velocity in liquid LBE for bubble equivalent diameter 4 mm to 6mm. The full squares and circles indicate the experimentally predicted value and the Harmathy empirical correlation Eq. (7) prediction. The dash line denotes the average value of experimental results. As can be seen, the single bubble terminal rising velocity obtained by the present study in liquid metal is about 0.252 m/s to 0.274 m/s and the corresponding Reynolds number is about 6707–9429. The Eötvos number is about 4.08–9.17 and the bubble terminal rising velocity tends to a value which is independent of the bubble equivalent diameter. It can be said the bubble flow located in the regime of surface tension dominant, which the bubble terminal rising velocity depends on the surface tension and inertia force. The dimensionless number G_1 is about 1.176×10^{-13} in liquid LBE, which is under the conditions of Harmathy empirical correlation Eq. (7). As shown in this figure, the experimental prediction of bubble terminal rising velocity in liquid metal are compared with the prediction by Harmathy empirical correlation. The figure indicates that the Harmathy empirical correlation can appropriately give the trend prediction reasonably well at single bubbly flow (equivalent diameter 4 mm–6 mm). On the other hand, the empirical correlation predicted value slightly underestimated the experimental terminal velocity. This may be due to the Harmathy empirical correlation was obtained by traditional fluids experiments which the surface tension and density of liquid are smaller than the liquid metal. It will produce larger buoyancy in liquid metal under bubble rising process. The single bubble rising velocity empirical correlation Eq. (7) can be modified as follows applied to liquid metal bubbly flow.

$$V_T = 1.89\left(\frac{g\sigma}{\rho_l}\right)^{0.25} \quad (3.10G_1^{-0.25} < Re \text{ or } 5.75 < G_2 \text{ and } 4\ mm < d_e < 6\ mm)$$
$$G_1 = \frac{g\mu_l^4}{\rho_l\sigma^3}, \quad G_2 = \frac{gr_b^4V_T^4\rho_l^3}{\sigma^3} \tag{13}$$

The small steam bubbles with equivalent diameter from 4 mm to 6 mm would therefore be entrapped and carried downward by the primary coolant flow when the coolant downward velocity is higher than the bubble terminal rising velocity (about 0.252 m/s to 0.274 m/s). It is suggested that the design of coolant circulation velocity is less than 0.252 m/s and the reactor geometry (particularly the downcomer region) is important to develop the prevention and mitigation of SGTR accident of lead-based reactor.

Based on wide-range database, the slight verification of the empirical correlation Eq. (13) and more accurate prediction methods for larger bubble diameter would be needed in future work.

Table 3
Values of drag coefficient in LBE.

Equivalent diameter (mm)	4.0	4.5	5.0	5.5	6.0
Drag coefficient	0.77	0.82	0.87	1.02	1.24

4. Conclusions

The single bubble terminal rising velocity in opaque liquid metal has been investigated by injecting argon gas into four transparent liquids (water, glycerol, alcohol and FC-3283). An appropriate modified correlation for single bubble rising velocity was recommended, which can roughly forecast the bubble rising velocity in gas-liquid metal bubbly flow. In the end, the suggestion for the reactor design of coolant velocity was given. The main results are as follows:

1. In liquid metal case since the density is very high, the single bubble shape in liquid LBE will be the ellipsoid transited to cap-shape or the cap-shape.
2. The drag coefficient of bubble flow in liquid is expressed as a function of dimensionless Eötvos number under different liquids. This method is based on the dimensionless Eötvos number which is related to the liquid surface tension, liquid density and bubble size. It is applied for two phase flow with high liquid-to-gas density ratio

to predict the bubble rising velocity.

3. For bubble equivalent diameter from 4 mm to 6 mm, the bubble flow in liquid metal located in the regime of surface tension dominant, and the surface tension and inertia force are the main influence factors for the bubble terminal rising velocity. The rising velocity tended to a constant value and it is almost independent of the bubble equivalent diameter.
4. The single bubble terminal rising velocity in opaque liquid metal remained around 0.252 m/s to 0.274 m/s for bubble equivalent diameter from 4 mm to 6 mm. The Harmathy empirical correlation predicted value slightly underestimated the experimental results and it was appropriately modified to apply to liquid metal bubbly flow.
5. It is suggested that the design of coolant circulation velocity is less than 0.252 m/s to develop the prevention and mitigation for the risk of steam migration in SGTR accident of lead-based reactor.

Acknowledgment

This work was supported by National Natural Science Foundation of China (Grant No. 11302224), Strategic Priority Science & Technology Program of the Chinese Academy of Sciences (Grant No. XDA03040000), National Magnetic Confinement Fusion Science Program of China (Grant Nos. 2014GB116000 and 2014GB112002). The authors would like to thank the great help from the other members of FDS team in this research.

Nomenclature

a	bubble minor axis (mm)
A	bubble cross-sectional area (mm^2)
b	bubble major axis (mm)
C_D	drag coefficient (−)
d_e	bubble equivalent diameter (mm)
d_n	nozzle diameter (mm)
Eo	Eötvos number = $g\rho_l d_e^2/\sigma$ (−)
E_r	relative error in measurement (−)
g	gravitational acceleration ($m{\cdot}s^{-2}$)
h	bubble rising height (mm)
G_1	dimensionless number = $g\mu_l^4/\rho_l\sigma^3$ (−)
G_2	dimensionless number = $gr_b^4V_T^4\rho_l^3/\sigma^3$ (−)
Mo	Morton number = $g\mu_l^4/\rho_l\sigma^3$ (−)
N	pixel amount in bubble spot
P_1 and P_2	the barycenter positions (pixel)
r_b	bubble radius (mm)
Re	Reynolds number = $\rho_l V_T d_e/\mu$ (−)
s	the scale factor (mm/pixel)
t	time of frame (s)
t_{tot}	the total measurement time (s)
$\triangle t$	the time between two images (s)
V	single bubble rising velocity ($m{\cdot}s^{-1}$)
V_t	single bubble terminal rising velocity ($m{\cdot}s^{-1}$)
V_b	bubble volume (mm^3)
X, Y	pixel coordinate of bubble barycenter (pixel)
x, y	each pixel position in bubble spot
z	vertical distance from the nozzle tip (mm)
z_{tot}	height of the liquid level (mm)

Greek symbols

μ	viscosity (Pa·s)
ρ	liquid density (kgm^{-3})
σ	surface tension (Nm^{-1})

Subscripts

b	bubble
e	equivalent
g	gas
i	ith pixel
l	liquid
n	nozzle
r	relative
tot	total

References

Celata, G.P., D'Annibale, F., Di Marco, P., et al., 2007. Measurements of rising velocity of a small bubble in a stagnant fluid in one-and two-component systems. Exp. Therm. Fluid Sci. 31 (6), 609–623.
Chakraborty, I., Biswas, G., Polepalle, S., et al., 2015. Bubble formation and dynamics in a quiescent high-density liquid. AIChE J. 61 (11), 3996–4012.
Cinotti, L., Smith, C.F., Sienicki, J.J., et al., 2007. The potential of the LFR and the ELSY project. Rev. Gen. Nucleaire (4), 30–39.
Cinotti, L., Smith, C.F., Sekimoto, H., et al., 2011. Lead-cooled system design and challenges in the frame of Generation IV International Forum. J. Nucl. Mater. 415 (3), 245–253.
Dinh, T.N., 2008. Multiphase flow phenomena of steam generator tube rupture in a lead-cooled reactor system: a scoping analysis. In: Societe Francaise D'Energie Nucleaire-international Congress on Advances in Nuclear Power Plants-ICAPP 2007, "The Nuclear Renaissance at Work", 13 May 2007 through 18 May 2007, Nice 2765-2775.
Frogheri, M., Alemberti, A., Mansani, L., 2015. The lead fast reactor: demonstrator (ALFRED) and ELFR design. Fast reactors and related fuel cycles: safe technologies and sustainable scenarios (FR13). In: Proceedings of an International Conference. vol. 1.
Grace, J.R., 1976. Shapes and velocities of single drops and bubbles moving freely through immiscible liquids. Chem. Eng. Res. Des. 54, 167–173.
Gu, Z., Wang, G., Bai, Y., et al., 2015. Preliminary investigation on the primary heat exchanger lower head rupture accident of forced circulation LBE-cooled fast reactor. Ann. Nucl. Energy 81, 84–90.
Harmathy, T.Z., 1960. Velocity of large drops and bubbles in media of infinite or restricted extent. AIChE J. 6 (2), 281–288.
Huang, Q.Y., 2017. Status and improvement of CLAM for nuclear application. Nucl. Fusion 57 (8), 086042.
Huang, Q., Li, J., Wu, Q., et al., 2011. Progress in development of CLAM steel and fabrication of small TBM in China. J. Nucl. Mater. 417 (1-3), 85–88.
Huang, Q., FDS Team, 2014. Development status of CLAM steel for fusion application. J. Nucl. Mater. 455 (1-3), 649–654.
Ishii, M., Chawla, T.C., 1979. Local Drag Laws in Dispersed Two-phase Flow. Argonne National Lab., IL (USA).
Kupferberg, A., Jameson, G.J., Eng, C., 1969. Bubble formation at a submerged orifice above a gas chamber of finite volume. Trans. Instn. Chem. Engrs 47, 241–250.
Mendelson, H.D., 1967. The prediction of bubble terminal velocities from wave theory. AIChE J. 13 (2), 250–253.
Mishima, K., Hibiki, T., Saito, Y., et al., 1999. Visualization and measurement of gas–liquid metal two-phase flow with large density difference using thermal neutrons as microscopic probes. Nucl. Instrum. Methods Phys. Res. Sect. A Accel. Spectrom. Detect. Assoc. Equip. 424 (1), 229–234.
Moisseytsev, A., Sienicki, J.J., 2008. Transient accident analysis of a supercritical carbon dioxide Brayton cycle energy converter coupled to an autonomous lead-cooled fast reactor. Nucl. Eng. Des. 238 (8), 2094–2105.
Peebles, F., Garber, H., 1953. Studies on the motion of gas bubbles in liquid. Chem. Eng. Prog. 49 (2), 88–97.
Pesetti, A., Del Nevo, A., Forgione, N., 2015. Experimental investigation and SIMMER-III code modelling of LBE–water interaction in LIFUS5/Mod2 facility. Nucl. Eng. Des. 290, 119–126.
Qiu, L.J., Wu, Y.C., Xiao, B.J., et al., 2000. A low aspect ratio tokamak transmutation system. Nucl. Fusion 40 (3Y), 629.
Saito, Y., Mishima, K., Tobita, Y., et al., 2005a. Application of high frame-rate neutron radiography to liquid-metal two-phase flow research. Nucl. Instrum. Methods Phys. Res. Sect. A Accel. Spectrom. Detect. Assoc. Equip. 542 (1–3), 168–174.
Saito, Y., Mishima, K., Tobita, Y., et al., 2005b. Measurements of liquid–metal two-phase flow by using neutron radiography and electrical conductivity probe. Exp. Therm. Fluid Sci. 29 (3), 323–330.
Sibamoto, Y., Kukita, Y., Nakamura, H., 2002. Visualization and measurement of subcooled water jet injection into high-temperature melt by using high-frame-rate neutron radiography. Nucl. Technol. 139 (3), 205–220.
Stokes, G.G., 1851. On the Effect of the Internal Friction of Fluids on the Motion of Pendulums. Pitt Press.
Suzuki, T., Tobita, Y., Kondo, S., et al., 2003. Analysis of gas-liquid metal two-phase flows using a reactor safety analysis code SIMMER-III. Nucl. Eng. Des. 220 (3), 207–223.
Tuček, K., Carlsson, J., Wider, H., 2006. Comparison of sodium and lead-cooled fast reactors regarding reactor physics aspects, severe safety and economical issues. Nucl. Eng. Des. 236 (14), 1589–1598.
Wang, S., Flad, M., Maschek, W., et al., 2008. Evaluation of a steam generator tube rupture accident in an accelerator driven system with lead cooling. Prog. Nucl. Energy 50 (2), 363–369.
Wang, M., Lian, C., Li, Y., et al., 2015a. Preliminary conceptual design of a lead–bismuth cooled small reactor (CLEAR-SR). Int. J. Hydrogen Energy 40 (44), 15132–15136.
Wang, M., Huang, H., Lian, C., et al., 2015b. Conceptual design of lead cooled reactor for hydrogen production. Int. J. Hydrogen Energy 40 (44), 15127–15131.

Wu, Y., 2009. Fusion-based hydrogen production reactor and its material selection. J. Nucl. Mater. 386, 122–126.
Wu, Y., 2016a. Design and R&D progress of China lead-based reactor for ADS research facility. Engineering 2 (1), 124–131.
Wu, Y., 2016b. CLEAR-S: an integrated non-nuclear test facility for China lead-based research reactor. Int. J. Energy Res. 40 (14), 1951–1956.
Wu, Y., FDS Team, 2006. Conceptual design activities of FDS series fusion power plants in China. Fusion Eng. Des. 81 (23), 2713–2718.
Wu, Y., FDS Team, 2007a. Conceptual design and testing strategy of a dual functional lithium–lead test blanket module in ITER and EAST. Nucl. Fusion 47 (11), 1533.
Wu, Y., FDS Team, 2007b. Design status and development strategy of China liquid lithium–lead blankets and related material technology. J. Nucl. Mater. 367, 1410–1415.
Wu, Y., FDS Team, 2007c. Design analysis of the China dual-functional lithium lead (DFLL) test blanket module in ITER. Fusion Eng. Des. 82 (15), 1893–1903.
Wu, Y., Huang, Q., Bai, Y., et al., 2010. Preliminary experimental study on the corrosion of structural steels in liquid lead bismuth loop. Chinese J. Nucl. Sci. Eng. 30 (3), 238–243.
Wu, Y., Jiang, J., Wang, M., et al., 2011. A fusion-driven subcritical system concept based on viable technologies. Nucl. Fusion 51 (10), 103036.
Wu, Y., Bai, Y., Song, Y., et al., 2014. Conceptual design of China lead-based research reactor CLEAR-I. Nucl. Sci. Eng. 34, 201–208.
Wu, Y., Wang, M., Huang, Q., 2015. Development status and prospects of lead-based reactors. Nucl. Sci. Eng. 35 (2), 213–221.
Wu, Y., Bai, Y., Song, Y., et al., 2016a. Development strategy and conceptual design of China lead-based research reactor. Ann. Nucl. Energy 87, 511–516.
Wu, Y., Chen, Z., Hu, L., et al., 2016b. Identification of safety gaps for fusion demonstration reactors. Nature Energy 1, 16154.
Ziqi, C., Yuyun, B., Zhengming, G., 2010. Hydrodynamic behavior of a single bubble rising in viscous liquids. Chin. J. Chem. Eng. 18 (6), 923–930.
Zrodnikov, A.V., Toshinsky, G.I., Komlev, O.G., et al., 2006. Nuclear power development in market conditions with use of multi-purpose modular fast reactors SVBR-75/100. Nucl. Eng. Des. 236 (14), 1490–1502.
Zrodnikov, A.V., Toshinsky, G.I., Komlev, O.G., et al., 2011. SVBR-100 module-type fast reactor of the IV generation for regional power industry. J. Nucl. Mater. 415 (3), 237–244.